

Modelling the impact of anthropogenic aerosols on CCN concentrations over a rural boreal forest environment

Supplementary material

5

Dry deposition of particles

10 The average deposition velocities over land and sea (with land-sea mask cut-off as 0.8 for land and 0.2 for sea) are shown in Fig 3, which also shows settling velocities from studies reported in Farmer et al. (2021) for forest land (Höfken and Gravenhorst, 1982; Grosch and Schmitt, 1988; Lorenz and Murphy, 1989; Waraghai and Gravenhorst, 1989; Gallagher et al., 1997; Gaman et al., 2004; Pryor, 2006; Grönholm et al., 2007; Pryor et al., 2008; Groenholm et al., 2009; Pryor et al., 2009; Vong et al., 2010; Gordon et al., 2011; Mammarella et al., 2011; Lavi et al., 2013; Zhang et al., 2014) and for water surfaces (Möller and Schumann, 1970; Sehmel, 1973; Caffrey et al., 1998; Zufall et al., 1998; 15 Qi et al., 2020). The rates in the model followed the same general profile with observations, where the minimum was around 0.2 cm m⁻¹ at 100 nm over land and 0.03 cm m⁻¹ at 200 nm over sea.

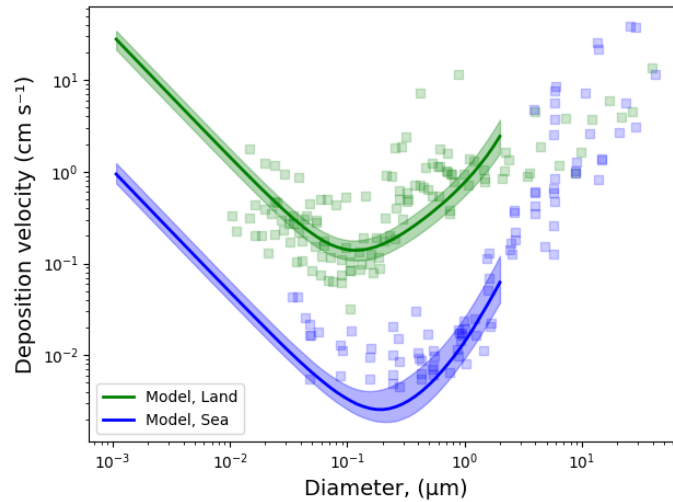


Figure S1: Median dry deposition velocities of aerosols in SOSAA over land (land-sea mask>0.8, green) and sea (land-sea mask<0.2, blue), with shaded interquartiles. The square markers are from Farmer et al. (2021), showing combined results from 16 (forest) and 5 (sea) studies.

20

SOSAA PreProcessor (SPP)

For a given gas compound or primary aerosol particle we get the average emissions $\langle E_\sigma \rangle$ from a given sector σ at time t with

$$\langle E_{t,\sigma} \rangle = \frac{E_{\sigma,t,k,j} SRR_{t,k,j}}{\sum_{k,j} SRR_{t,k,j}} \quad (1)$$

25 where t , k and j are the time, and latitude and longitude grid indices, respectively. The mean emission E is a representation of the average emissions affecting the airmasses at that time. The CAMS emissions are provided as mean of different timescales and amended with temporal profiles (diurnal and/or weekly), which are applied by SPP based on

the emission source sectors, times and locations of the SRR weight factors. Anthropogenic emissions also have a vertical profile, and here we followed the method in EMEP MSC-W chemical transport model (Simpson et al., 2012) and used a spatio-temporally constant but sector dependent 12-layer profile for all emissions from CAMS-ANT and GAINS particles, extending from 0 to 900 metres above the ground. In this study we summed all the sector specific emissions before using it as input in SOSAA, therefore following Eq. 1 the final emissions for a given compound along a trajectory is obtained by

$$\langle E_t \rangle = \sum_{\sigma} V_{\sigma} \langle E_{t,\sigma} \rangle \quad (2)$$

where V_{σ} is the vertical profile for sector σ . The output of SPP is a NetCDF file with emission rates (in $\text{kg m}^{-2} \text{s}^{-1}$) of the processed compounds as trajectories, separate for each emission dataset. The names of the emitted gaseous compounds in CAMS and their counterpart in the chemistry scheme are shown in Table S1.

Table S1: CAMS global emission variables and the compounds they were associated in SOSAA chemistry. Note the SO_2 emission reduction factor 0.5. Data sources: A= GAMS-GLOB-ANT, B= GAMS-GLOB-BIO.

Name in CAMS datasets	MCM long name	in chemistry	Source in CAMS	Fraction (mass)
hexanes	HEXANE (N-HEXANE)	NC6H14	A	
butanes	N-BUTANE	NC4H10	A	
pentanes	PENTANE (N-PENTANE)	NC5H12	A	
propane	PROPANE	C3H8	A	
other-VOCs	Not used	Not used	A	
ethane	ETHANE	C2H6	A	
benzene	BENZENE	BENZENE	A	
ethene	ETHENE (ETHYLENE)	C2H4	A	
xylylene	1,2-DIMETHYL BENZENE (O-XYLENE)	OXYL	A	0.33
-:-	1,3-DIMETHYL BENZENE (M-XYLENE)	MXYL	A	0.33
-:-	1,4-DIMETHYL BENZENE (P-XYLENE)	PXYL	A	0.33
alcohols	METHANOL	CH3OH	A	0.2
-:-	ETHANOL	C2H5OH	A	0.2
-:-	1-PROPANOL (N-PROPANOL)	NPROPOL	A	0.3
-:-	2-PROPANOL (I-PROPANOL)	IPROPOL	A	0.3
other-alkanes-and-alkynes	Not used	Not used	A	
other-aromatics	ETHENYL BENZENE (STYRENE)	STYRENE	A	
toluene	METHYLBENZENE (TOLUENE)	TOLUENE	A	
other-aldehydes	ETHANAL (ACETALDEHYDE)	CH3CHO	A	
acetylene	ETHYNE (ACETYLENE)	C2H2	A	
propene	PROPENE (PROPYLENE)	C3H6	A	
formaldehyde	METHANAL (FORMALDEHYDE)	HCHO	A	
trimethylbenzene	1,2,3-TRIMETHYL BENZENE (HEMIMELLITENE)	TM123B	A	0.33
-:-	1,2,4-TRIMETHYL BENZENE (PSEUDOCUMENE)	TM124B	A	0.33
-:-	1,3,5-TRIMETHYL BENZENE (MESITYLENE)	TM135B	A	0.33
total-ketones	PROPANONE (ACETONE)	CH3COCH3	A	
esters	METHYL FORMATE	CH3OCHO	A	
ethers	DIMETHYL ETHER	CH3OCH3	A	
total-acids	METHANOIC ACID	HCOOH	A	
monoterpenes	ALPHA-PINENE	APINENE	A	0.38
-:-	BETA-PINENE	BPINENE	A	0.27
-:-	LIMONENE	LIMONENE	A	0.09
-:-	-	CARENE	A	0.17
-:-	-	SABINENE	A	0.1
isoprene	2-METHYL-1,3-BUTADIENE (ISOPRENE)	C5H8	A	
methanol	METHANOL	CH3OH	B	
other-monoterpenes	LIMONENE	LIMONENE	B	0.25
-:-	-	CARENE	B	0.48
-:-	-	SABINENE	B	0.28
acetone	PROPANONE (ACETONE)	CH3COCH3	B	
pinene-a	ALPHA-PINENE	APINENE	B	
pinene-b	BETA-PINENE	BPINENE	B	
isoprene	2-METHYL-1,3-BUTADIENE (ISOPRENE)	C5H8	B	
ethene	ETHENE (ETHYLENE)	C2H4	B	
propene	PROPENE (PROPYLENE)	C3H6	B	
ethanol	ETHANOL	C2H5OH	B	
acetaldehyde	ETHANAL (ACETALDEHYDE)	CH3CHO	B	

sesquiterpenes	BETA-CARYOPHYLLENE	BCARY	B	
butenes-and-higher-alkenes	1-BUTENE	BUT1ENE	B	0.5
-:-	1-PENTENE	PENT1ENE	B	0.3
-:-	1-HEXENE	HEX1ENE	B	0.2
formaldehyde	METHANAL (FORMALDEHYDE)	HCHO	B	
other-aldehydes	ETHANAL (ACETALDEHYDE)	CH3CHO	B	0.7
-:-	PROPANAL (PROPRIONALDEHYDE)	C2H5CHO	B	0.3
toluene	METHYLBENZENE (TOLUENE)	TOLUENE	B	
other-ketones	BUTANONE (METHYL ETHYL KETONE)	MEK	B	
MBO	2-METHYL-3-BUTEN-2-OL	MBO	B	
hydrogen-cyanide	-	-	B	
methyl-choride	CHLOROMETHANE (METHYL CHLORIDE)	CH3CL	B	
ethane	ETHANE	C2H6	B	
methyl-bromide	BROMOMETHANE	CH3BR	B	
methyl-iodide	-	CH3I	B	
propane	PROPANE	C3H8	B	
Butanes-and-higher-alkanes	N-BUTANE	NC4H10	B	
CH ₄	METHANE	CH4	B	
DMS	DIMETHYL SULPHIDE	DMS	B	
CO	CO	CO	B	
CH ₄	METHANE	CH4	A	
SO ₂	SO2	SO2	A	0.5
NH ₃	No chemical reactions; only used in clustering with H ₂ SO ₄	NH3	A	
NO _x	NO	NO	A	0.2
-:-	NO2	NO2	A	0.8
CO	CO	CO	A	

40 Kappa parameters for CCN

Table S2: κ values used to calculate CCN concentration. Range estimation was done by adding the upper or lower limits (shown in parenthesis) to nominal κ . The upper and lower range were chosen from the spread in κ estimations in literature, (references in “Comment”).

Composition	κ_c	Comment
Primary particles	0.208 (-0.1, +0.2)	levoglucosan ($\kappa=0.208$) (Petters and Kreidenweis, 2007)
Secondary organics	0.15 (-0.1, +0.1)	Adapted from Paramonov et al. (2013), who report values between 0.1 and 0.2 for high organic fractions.
Sea salt	1.28 (-0.1, +0.2)	(Petters and Kreidenweis, 2007). This value has been shown to be too small (Paramonov et al., 2013)
Sulfuric acid	1.0 (-0.2, +0.2)	J. Schmale et al., ideal case
Molecular clusters	0.9 (-0.3, 0)	Ammonium bisulfate (Petters and Kreidenweis, 2007)

Statistical descriptors

Normalized Mean Bias Factor (B_{NMBF} , Yu et al., 2006):

$$B_{\text{NMBF}} = \frac{\sum_i M_i}{\sum_i O_i} - 1, \text{ when } \bar{M} \geq \bar{O} \quad , \quad B_{\text{NMBF}} = [-\infty, \infty]$$

$$1 - \frac{\sum_i O_i}{\sum_i M_i}, \text{ when } \bar{M} < \bar{O}$$
(3)

45

Mean Factor Bias and Mean Factor Error (EPA, 2007):

$$MFB = \frac{2}{N} \frac{\sum_N (M_i - O_i)}{\sum_N M_i + O_i} \times 100\%, [-200\%, 200\%]$$
(4)

$$MFE = \frac{2}{N} \frac{\sum_N |M_i - O_i|}{\sum_N M_i + O_i}, [0, \infty] \quad (5)$$

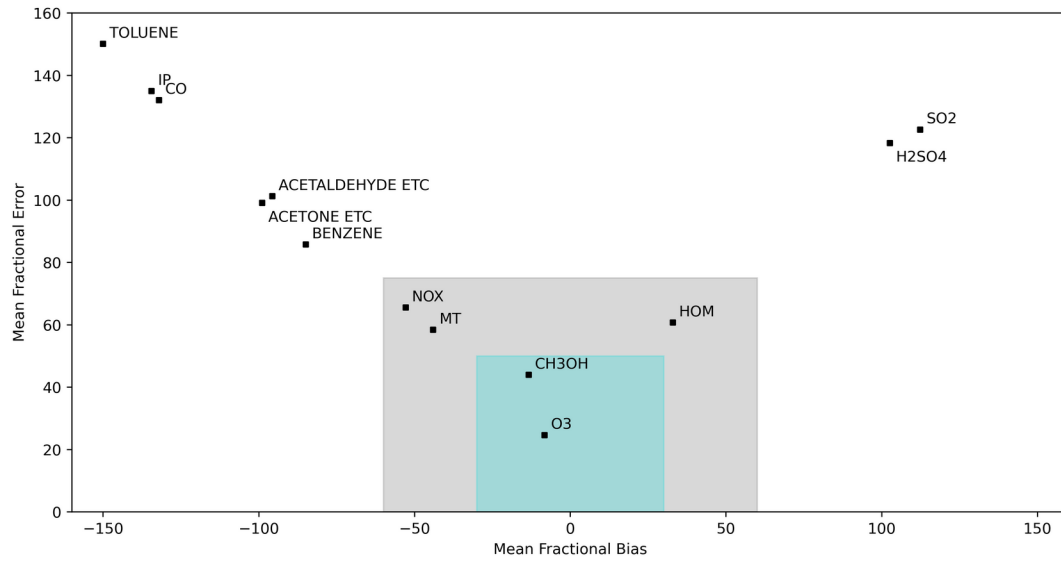


Figure S2: Daily median MFB and MFE in an EPA model evaluation criteria field.

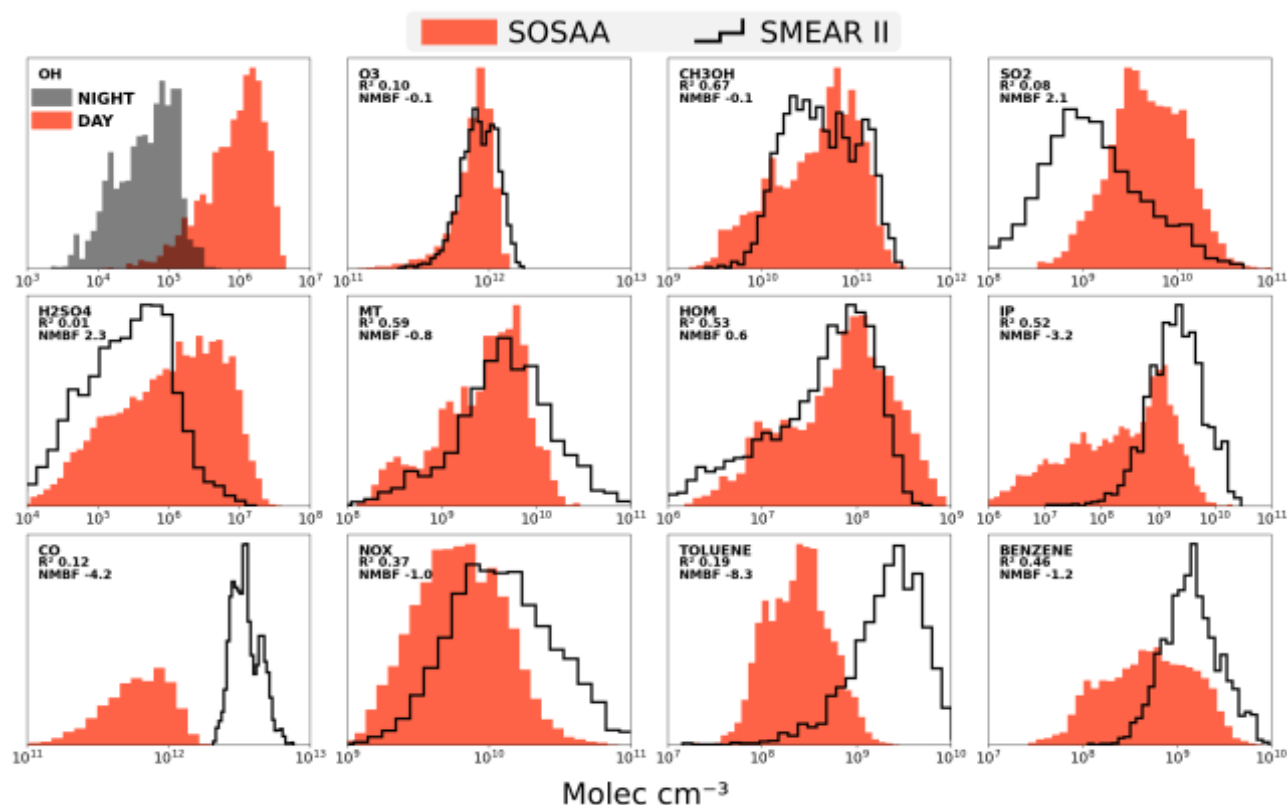


Figure S3: Distributions of gas concentrations during Mar-Oct 2018 in SOSAA model and SMEAR II measurements.

Modelled CCN number concentrations, critical diameters and κ

Table S3: Mean CCN number concentration, critical dry diameter D_{crit} , κ at D_{crit} and mean κ of $CCN > D_{crit}$ for the modelled supersaturation classes. Figures in parentheses show the minimums and maximums calculated using the range of κ shown in Table S2.

Supersaturation	NC (cm ⁻³)	Critical dry diameter (nm)	Critical κ	Mean κ
0.1 %	193 (171–225)	176.0 (155.7–193.0)	0.330 (0.258–0.468)	0.275 (0.232–0.370)
0.2 %	339 (315–374)	111.3 (99.6–120.9)	0.328 (0.263–0.450)	0.255 (0.208–0.352)
0.4 %	512 (488–546)	70.2 (63.7–75.3)	0.329 (0.274–0.433)	0.246 (0.198–0.342)
0.6 %	629 (607–661)	53.6 (49.1–57.0)	0.331 (0.282–0.424)	0.243 (0.195–0.338)
0.8 %	720 (700–750)	44.3 (40.8–46.9)	0.332 (0.287–0.417)	0.241 (0.193–0.336)
1.0 %	796 (772–824)	38.2 (35.3–40.3)	0.332 (0.290–0.412)	0.240 (0.192–0.334)
1.2 %	861 (835–888)	33.9 (31.4–35.7)	0.331 (0.292–0.408)	0.239 (0.192–0.333)

50

Impact of H₂SO₄, NH₃ CS and Temperature in cluster formation rates from ACDC

Figure S7 shows the averaged changes in cluster formation rates along the trajectories in the ZeroPNE compared to BASE. As the coagulation sink generally decreased, the effect was on average approximately threefold increase in new particle formation. Notably, at time periods when the model and observations showed low concentrations in the nucleation modes (July and early September), ZeroPNE showed up to tenfold increase in cluster formation rates, indicating that the primary emissions were heavily suppressing the cluster formation in those time periods.

55

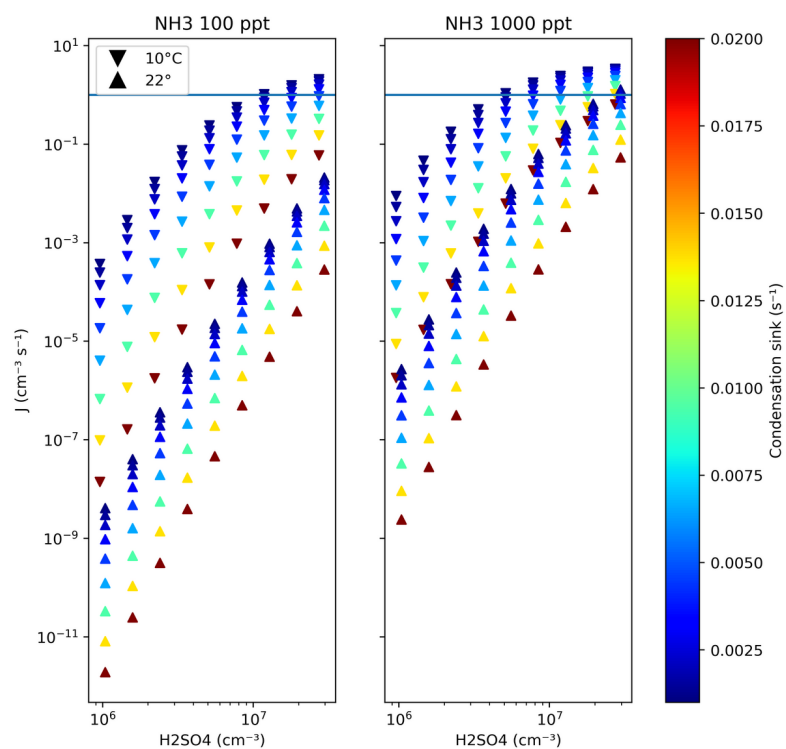


Figure S4: Sensitivity of the $\text{H}_2\text{SO}_4\text{-NH}_3$ chemistry in ACDC to key parameters: monomer concentrations, condensation sink (which is used to scale the coagulation sink of the interstitial clusters) and temperature. These values are from steady state simulations. The blue line marks $1 \text{ cm}^{-3} \text{ s}^{-1}$.

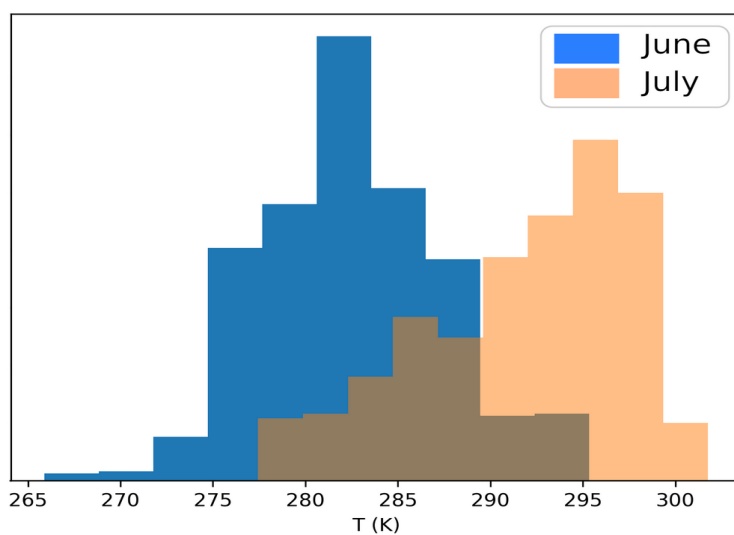


Figure S5: Mean 8 am temperatures along the trajectory between 0–96 hours.

Figures 4 and 5 show the effect of condensation sink and temperature to formation rate as function of monomer concentrations. The temperatures (10°C and 22°C) were selected to represent the mode of the temperatures at 8 am (UTC, these are not necessarily local times) along the trajectories in June (10°C) and July (12°). Even at 1 ppb ammonia and $3 \times 10^7 \text{ H}_2\text{SO}_4$ concentrations, at 22°C and high condensation sink, the nucleation rates fall well below $1 \text{ cm}^{-3} \text{ s}^{-1}$.

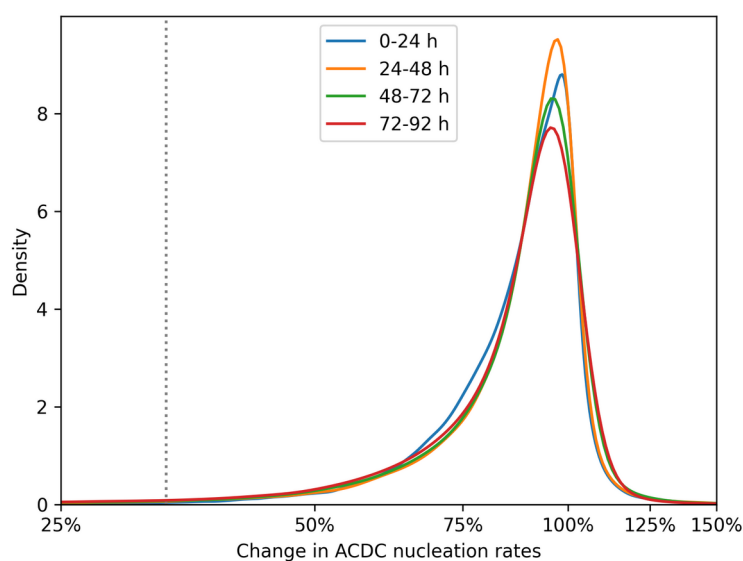


Figure S6: Change in ACDC nucleation module due to multiplying the cluster formation rates outside ACDC by a factor of 3. The dashed vertical line shows approximately 33% limit, where the multiplication factor is being offset by decrease in ACDC due to increased condensation sink. The mean value of these distributions (0.873) was used to correct the f_I in the response analysis (leading to $f_I=2.62$).

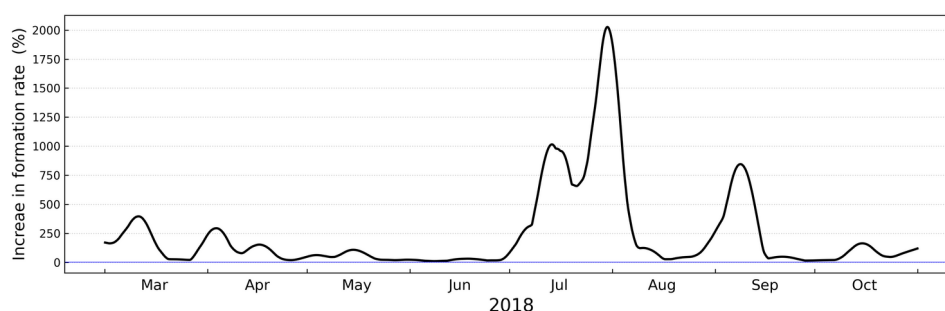


Figure S7: 12 day running mean of the enhancement of nucleation rates calculated by ACDC when primary particle emissions were turned off. The data was calculated from the ratio of the mean nucleation rates for the last 96 hours along the trajectory for ZeroPNE and BASE, then a running mean smoothing was applied. The largest increases in nucleation rates coincide with the peaks in the response of modelled CCN 1.0% to the primary particles.

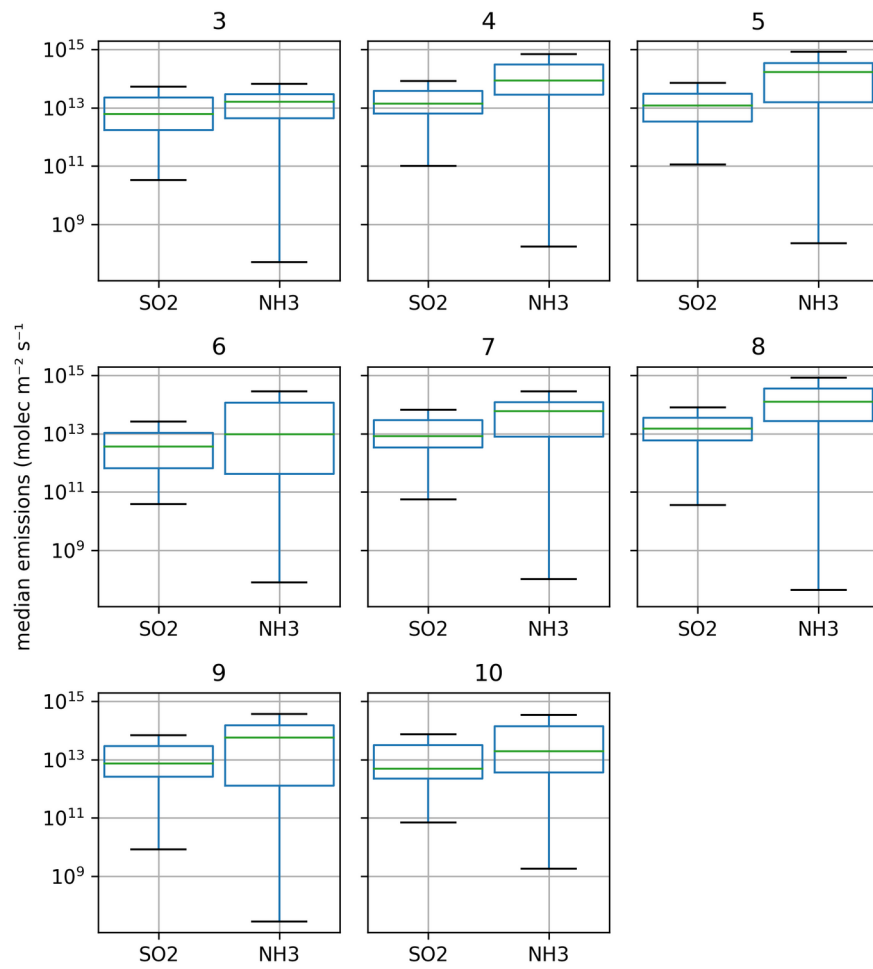


Figure S8: Median SO_2 and NH_3 emissions along trajectory (last 4 days) by month (3=Mar, 10=Oct).

Particle size distributions

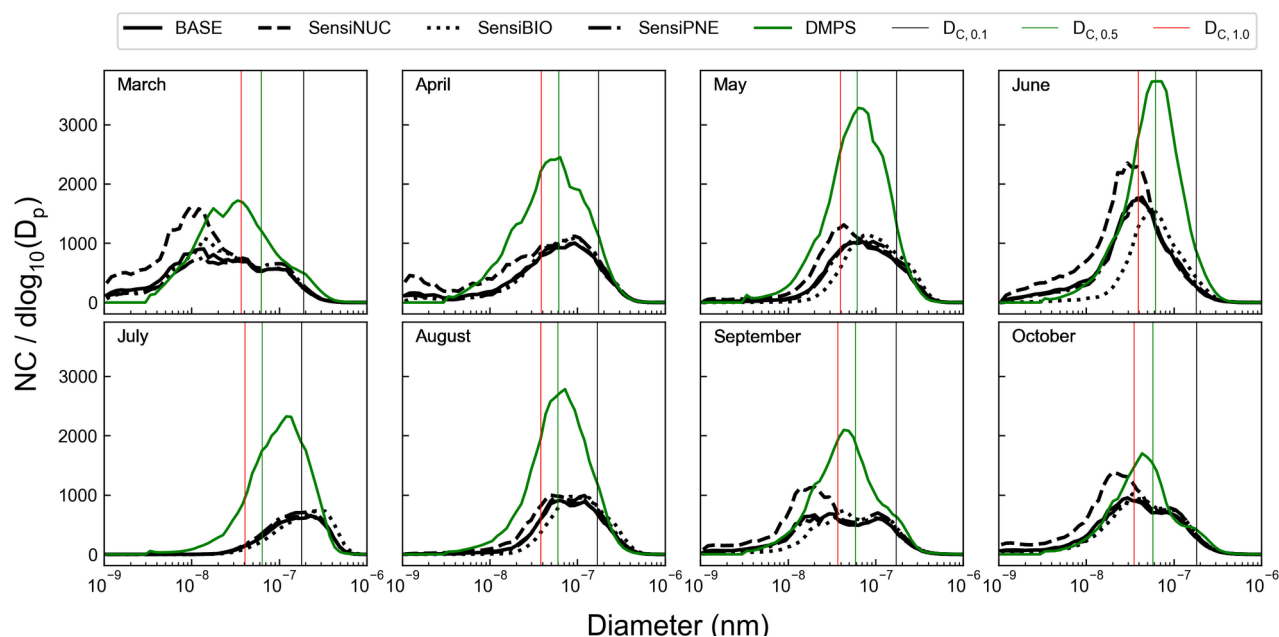


Figure 9: Median measured (DMPS) and modelled (“BASE” and “Sensi”-simulations, Table 2 in the main article) particle size distributions at the station by month for the study period. Vertical lines show the median critical dry diameters of 0.1%, 0.5% and 1.0% supersaturation.

Applied reduction in GAINS number and sea salt particle emissions

Initial simulations showed overestimation in the PM₁, along with overestimation in the coarse mode number concentrations. This seemed to be due to primary number emissions (PNE and sea salt). The problem with the relatively coarse classification of the GAINS size distribution meant that mass emissions are sensitive to how the smoothing was done, as the choice of the mass mean diameter (MMD) of the uniformly distributed bins affects total mass. Furthermore, GAINS number emissions are not necessarily mass consistent. A few percent difference in the total number concentration, if applied to the largest bins, will change the total mass substantially. For these reasons, the coarse mode emissions of both sea salt and primary number emissions were multiplied with a time-invariant function that reduced the number emissions, starting from 230 nm diameter with 5% reduction, through 50% reduction in 330 nm diameter and finally 93% reduction in 1 μm diameter particle number emissions. This resulted in approximately 2% reduction in total number emissions and approximately 55% reduction in PM₁ mass emissions, varying somewhat with the emission size distribution.

How well do the responses predict changes in extreme case?

70 The response to CCN was calculated using a relatively small perturbation of model input and relating it to the change in the model CCN output. But how well does the response predict model response in case of large perturbation to the tested input? We defined the response as a linear function, because $Q_P = Q_B[R(f_I-1)+1]$, where we assume that R and f_I both stay constant with respect to Q_B – acknowledging that both assumptions are idealizations of the real conditions. With these assumptions, when $f_I = 0$, meaning that the process in question is completely removed, Q_P is due to contributions of other processes in the model. In this case $Q_P = Q_B(1-R)$. We tested this prediction with the ZeroAER and ZeroNUC cases by comparing the prediction of the linear model to the actual model results in the Zero cases. It turns out that the linearity is a good approximation even in the extreme case of $f_I=0$ for the primary particle emissions, but a bad approximation for the nucleation rates. Here we expand the linear form of R by noticing that the both terms in the right hand side rational function in Eq. (6) are linear approximations of the logarithm. This implies that the output factor f_Q in the model is the input factor f_I to the power of the response R :

$$R_{POW} = \frac{\ln(f_Q)}{\ln(f_I)} \rightarrow f_Q = f_I^{R_{POW}} = Q_P = Q_B f_I^{R_{POW}} \quad (6)$$

The problem with this model is that $f_Q \rightarrow 0$ when $f_I \rightarrow 0$, in effect neglecting other processes that contribute to the CCN NC, so we expand the equation to

$$Q_P = (Q_0 + Q_{NUC}) f_I^{R_{POW}} = Q_0 + Q_{NUC} f_I^{R_{POW}} \quad (7)$$

Where we define Q_0 as the part of Q_B for which $R=0$, meaning it is invariant to the process that is varied. Here the invariant part Q_0 is what the ZeroNUC solves. If we equate $CCN_{ZeroNUC}$ with Eq. (6), we can estimate the largest f_I which approximates $CCN_{ZeroNUC}$ (by minimizing the model bias, for example). We found that in CCN supersaturation classes 0.1–0.2% reducing the nucleation rates by a factor of 100, the effect of nucleation to was in practice completely removed ($B_{NMBF} < 1\%$). In smaller CCN sizes, the nucleation rates would have to be reduced by a factor of 10^{-4} . Figure S10 shows the prediction of CCN number concentrations made with the linear function in case of primary particle emissions and nucleation, and in addition power law function in case of nucleation (using a constant $f_I=10^{-3}$). The linear function fails completely to predict the effect of reduced nucleation, but fairs much better with the primary emissions. For consistency, Figure S10 also shows the f_I which would minimize the bias in the power law model in the PNE cases. These factors were unrealistically high, at least 0.1, but the simpler linear model gave adequate predictions with the actual $f_I=0$. In all cases, the response was a useful metric to estimate the number concentrations even in the extreme case of turning off the process altogether. Figure S11 shows the same data in a time series, with red (blue) shading showing over(under)estimation by the respective model when compared with the Zero cases.

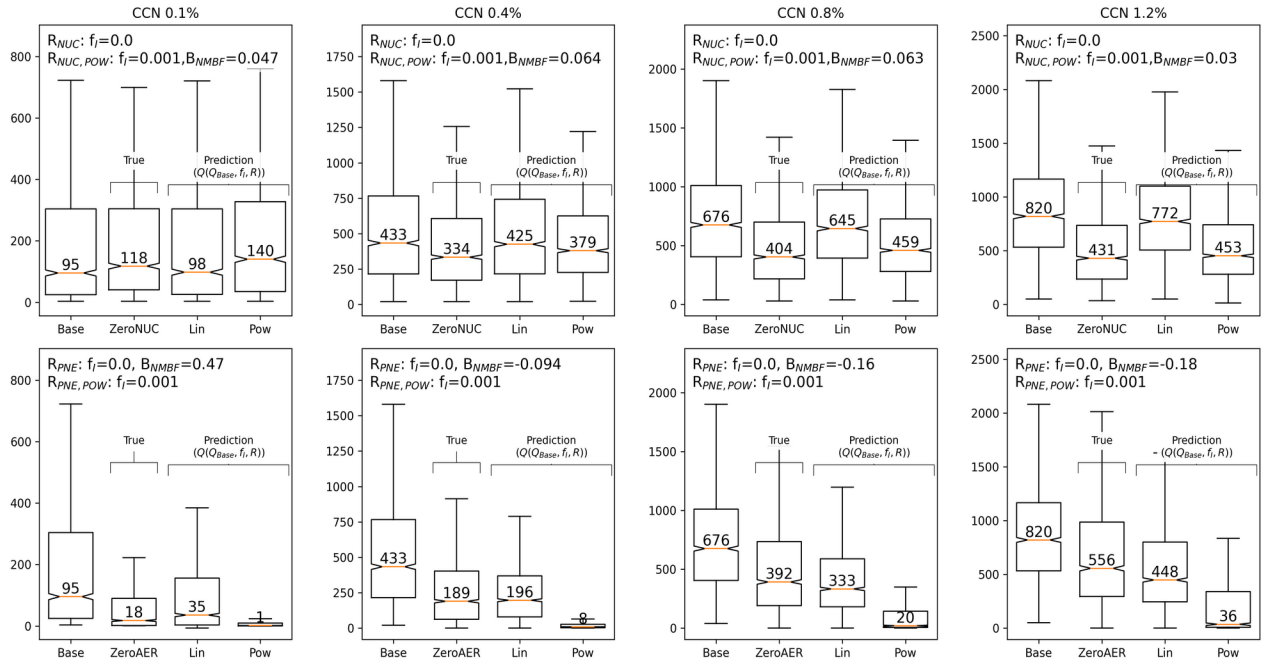


Figure S10: Boxplots of the CCN number concentrations of 0.2%, 0.4% and 1.0% supersaturation classes from the Base and Zero simulations (3-hourly, 8-months times series), and the prediction of CCN in a case where NUC or PNE would be turned off ($f_i=0.0$, Lin), or multiplied with a factor $f_i=0.001$ (Pow). Predictions were obtained by using the Base concentrations, CCN responses and the multiplication factor f_i . The B_{NMBF} of the Pow and Lin predictions is shown for NUC and PNE, respectively.

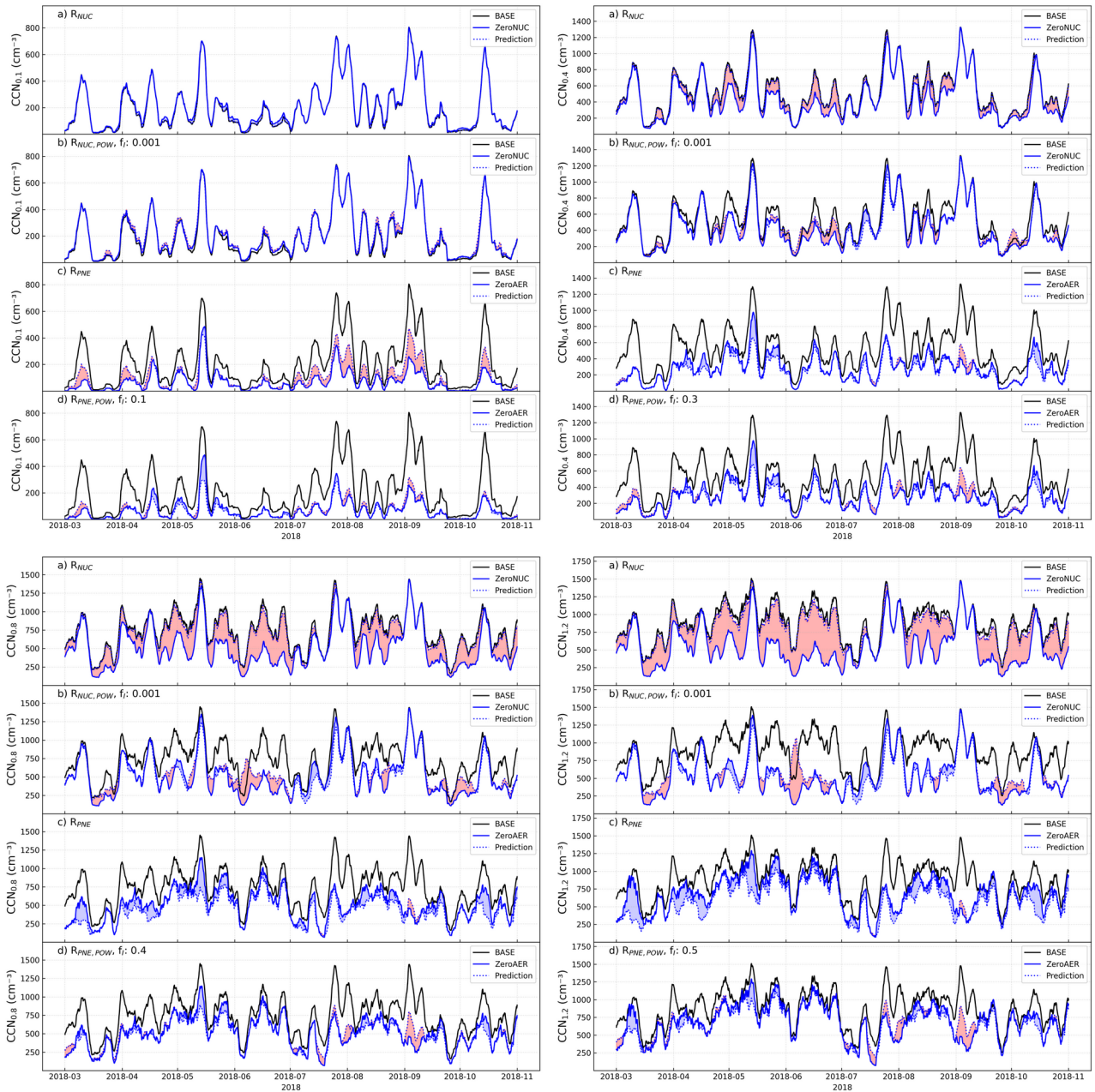


Figure S11: Time series of the CCN number concentrations of 0.2%, 0.4% and 1.0% supersaturation classes from the Base and Zero simulations (3-hourly, 8-months times series), and the prediction of CCN in a case where NUC or PNE would be turned off ($f_1=0.0$, Lin), or multiplied with a factor $f_1=0.001$ (Nuc,Pow). RPNE,POW uses a multiplication factor that minimizes the bias.

In conclusion, the responses calculated with perturbing the model can be used to estimate the overall contribution of the tested process. The primary emissions seem to follow the linear model better, whereas the effect of the nucleation rate is better described with the power law model. If this behaviour also holds with significantly increased nucleation rates, the low responses which appear in the exponent, mean that the CCN number concentration is rather insensitive to changes in the formation rates, at least to anything less than a magnitude. This does not imply that nucleation is unimportant, as the responses are reflecting the overall state of the system and the impact of other, possibly dominating processes. This is evident in the 8-month time series of the size distribution surface plots which shows the ZeroNUC and ZeroPNE cases; without the suppression of primary emissions, new particle formation is still able to capture general form of the observed size distribution, but with some underestimation of the accumulation mode (Figure S13). To estimate the

suppressing effect of the combined NUC and PNE to the CCN concentrations, we compare the summed CCN from the Zero-simulations against BASE ($MD(\frac{\sum [CCN]_{ZERO}}{[CCN]_{BASE}})$). For supersaturation classes 0.2%–1.2% the median ZeroNUC+ZeroPNE concentrations were ca. 28% above BASE, while the median of summed $[CCN_{0.1\%}]$ was ca. 45% higher than BASE. These findings are consistent with the sensitivity studies which showed the negative impact of cluster formation rates to $[CCN_{0.1\%}]$.

We calculated projections of the average impact of new particle formation, or specifically the nucleation rates, and primary number emissions to CCN, for a range of scenarios where the processes change by a factor (Figure S12). This reflects the sensitivity simulations well; while increasing nucleation rates will produce a lot more particles in the nucleation mode, this effect gets faded when considering the larger particle sizes where the CCN is found. The effect of new particle formation is dependent on the growth of the particles, and this is dependent on the condensation of organic and inorganic compounds. Figure S12 also includes the projections for the change of CCN with respect to biogenic emissions (both the linear and exponential response is shown). Naturally, these projections are simplistic in the sense that parameters are scaled uniformly, meaning all BVOC and all PNE sizes are scaled with the same factor. In real scenarios, such changes would affect the shape of the size distributions and not only the overall fluxes, similarly changes in the chemical distribution of the biogenic emissions could change the response.

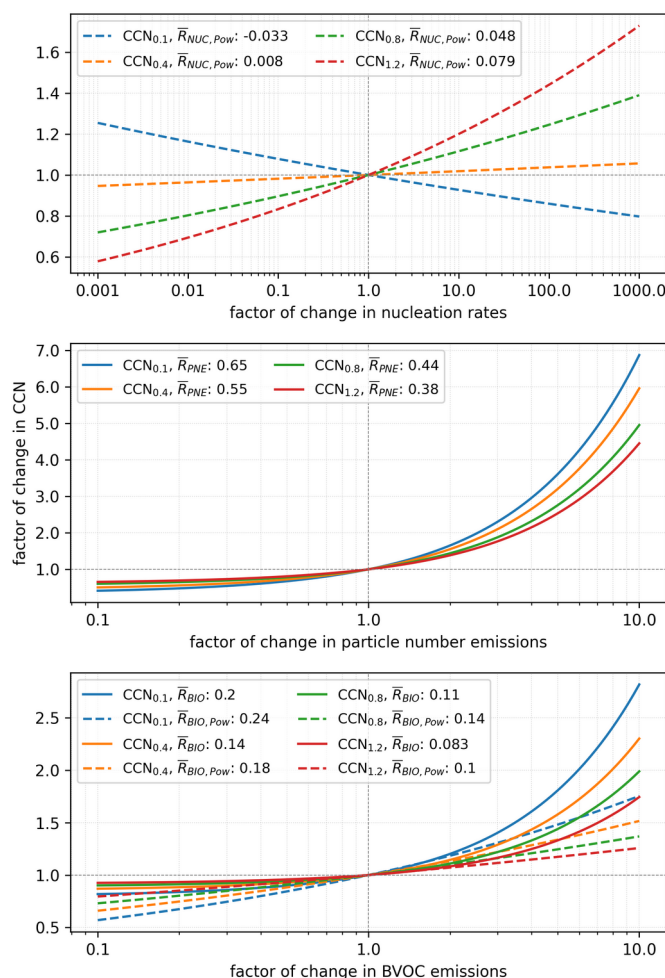
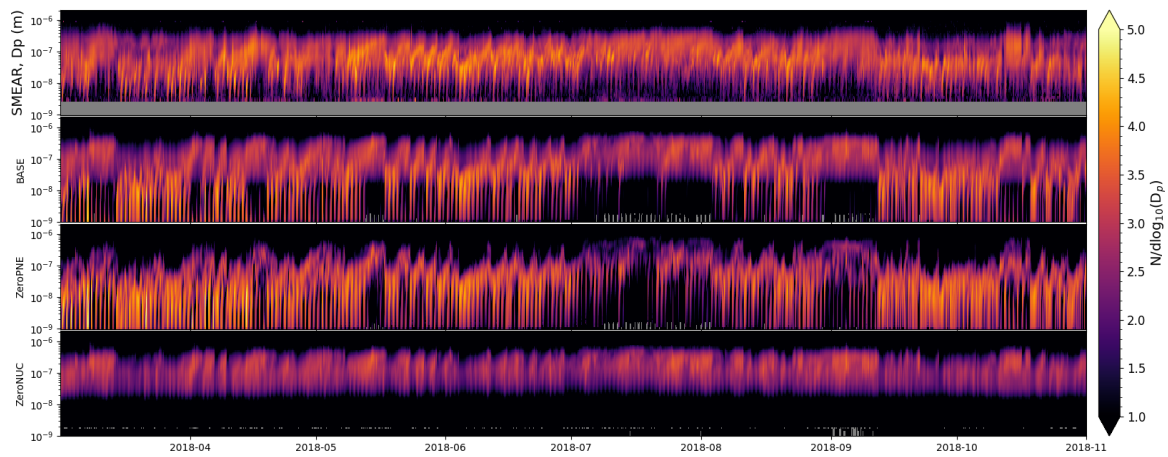


Figure S12: Projections of change in CCN as a response to change in nucleation rates, primary number and BVOC emissions, based on the calculated responses from the sensitivity runs. Note the different scales in the axes of the three panels.



130 *Figure S13: Measured (DMPS) and modelled particle number size distributions from the BASE, ZeroPNE and ZeroNUC simulations.*

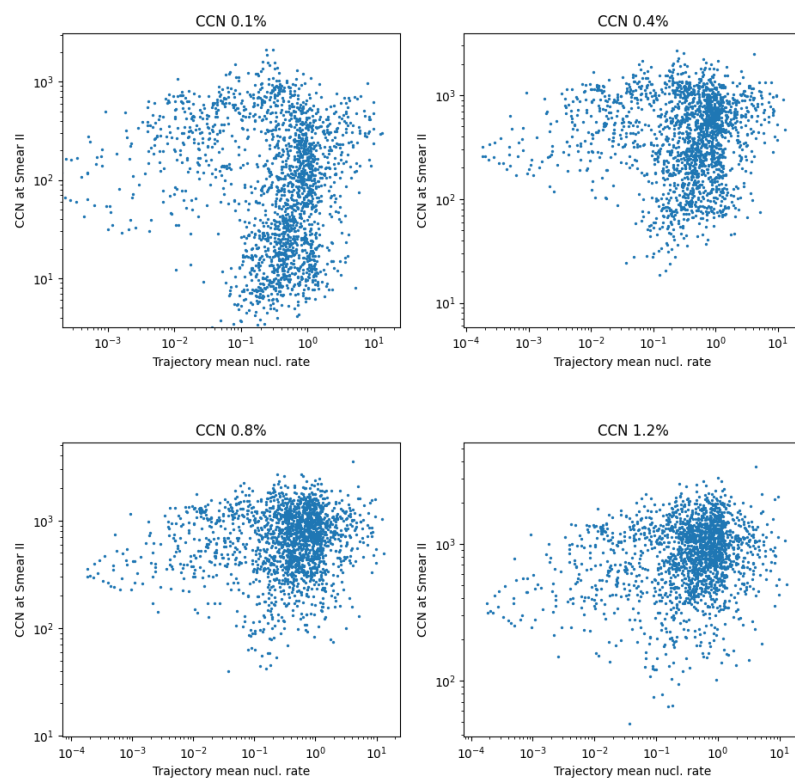


Figure S14: Scatter plot of modelled CCN at SMEAR II and mean cluster formation rate along the trajectories (0–4 days prior to SMEAR II).

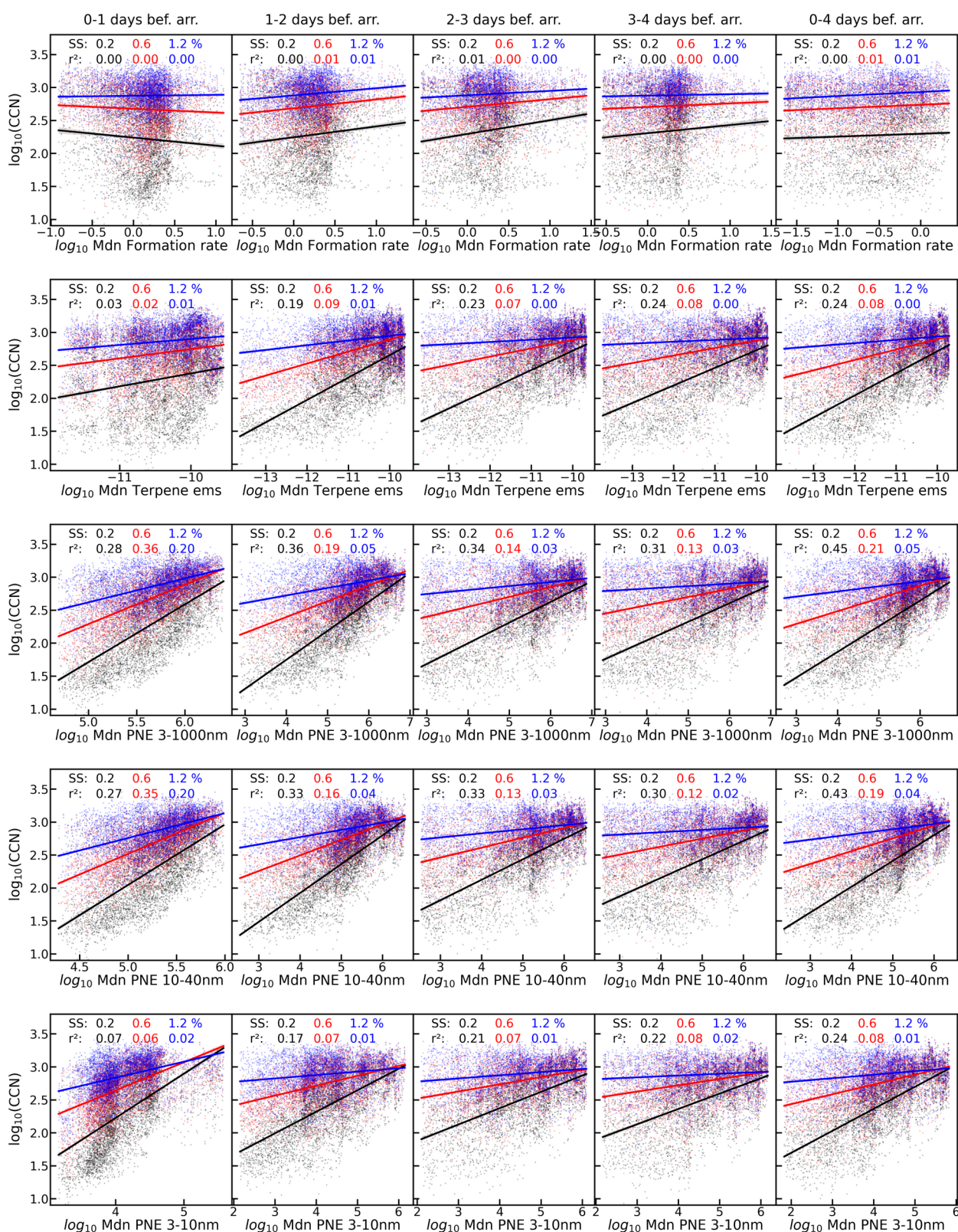


Figure S15: Scatter plots of modelled CCN at the station and various model parameters, correlating CCN at the station and the history of the parameter state along trajectories. Columns show median values of emissions and cluster formation rates 0–1, 1–2, 2–3 and 3–4 days before the trajectory arrives at the station.

Table S4: Relative change in modelled median of CCN number concentration in the two Zero-runs compared with BASE, one where primary anthropogenic particle emissions were turned off, and one where cluster formation (nucleation) was turned off. The 95% confidence intervals are calculated by bootstrapping with 50000 samplings. This table corresponds to data in Figs. 12 and 13 in the main article.

CCN	All months		Spring		Summer		Autumn	
Primary particle emissions set to zero (ZeroPNE)								
0.1%	-82%	(-86,-78)%	-87%	(-91,-83)%	-76%	(-80,-71)%	-89%	(-96,-80)%
0.4%	-56%	(-60,-53)%	-59%	(-67,-54)%	-47%	(-53,-42)%	-60%	(-64,-55)%
0.8%	-42%	(-45,-38)%	-42%	(-47,-37)%	-37%	(-42,-33)%	-48%	(-53,-42)%
1.2%	-33%	(-36,-29)%	-32%	(-38,-26)%	-32%	(-38,-26)%	-35%	(-40,-28)%
Cluster formation set to zero (ZeroNUC)								
0.1%	+23%	(+12,+35)%	+35%	(+13,+58)%	+14%	(+2,+33)%	+36%	(+16,+70)%
0.4%	-22%	(-27,-18)%	-20%	(-29,-14)%	-21%	(-29,-16)%	-25%	(-35,-17)%
0.8%	-40%	(-43,-37)%	-35%	(-40,-29)%	-41%	(-45,-38)%	-43%	(-49,-38)%
1.2%	-48%	(-50,-45)%	-42%	(-47,-36)%	-50%	(-53,-47)%	-50%	(-55,-45)%

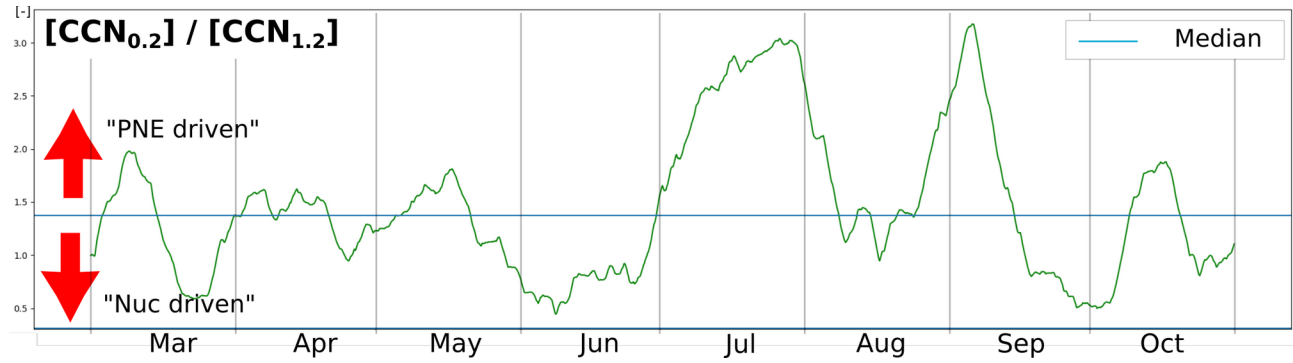


Figure 16: Ratios of $CCN_{0.2}/CCN_{1.2}$.

140

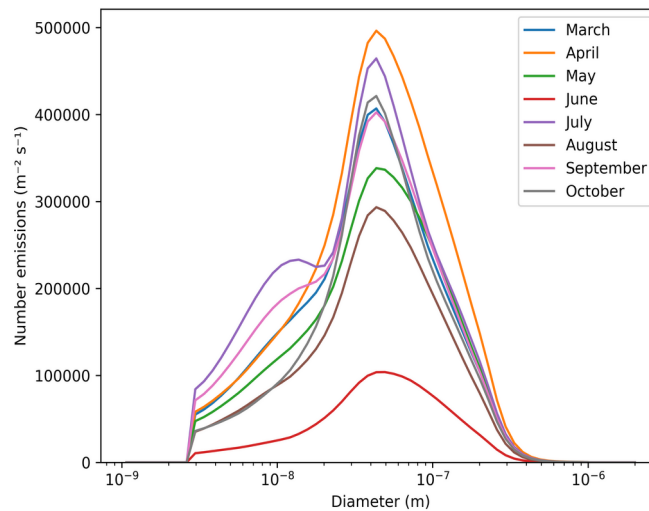


Figure 17: Mean size distributions particle number emissions along the trajectories by month.

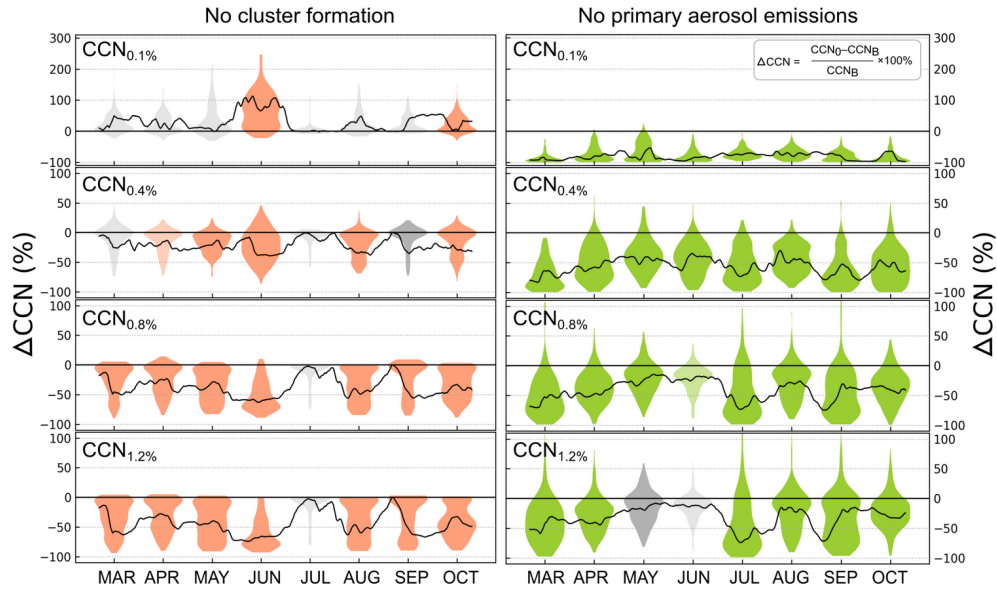


Figure 18: Distributions of the monthly relative changes in CCN concentrations in two model runs ZeroNUC (left panel) and ZeroPNE (right panel), aggregated from the 3-hourly modelled CCN concentration at the end of the trajectory. Coloured distributions have $p\text{-value} < 0.01$ in the Mood's median test, while light coloured data has $0.01 < p \leq 0.05$. For gray and light gray distributions $0.1 \geq p > 0.05$ and $p > 0.1$, respectively. The black line shows the 12-day running median of the relative difference in CCN concentrations between Zero-simulations and BASE. This figure corresponds to data in Table S4.

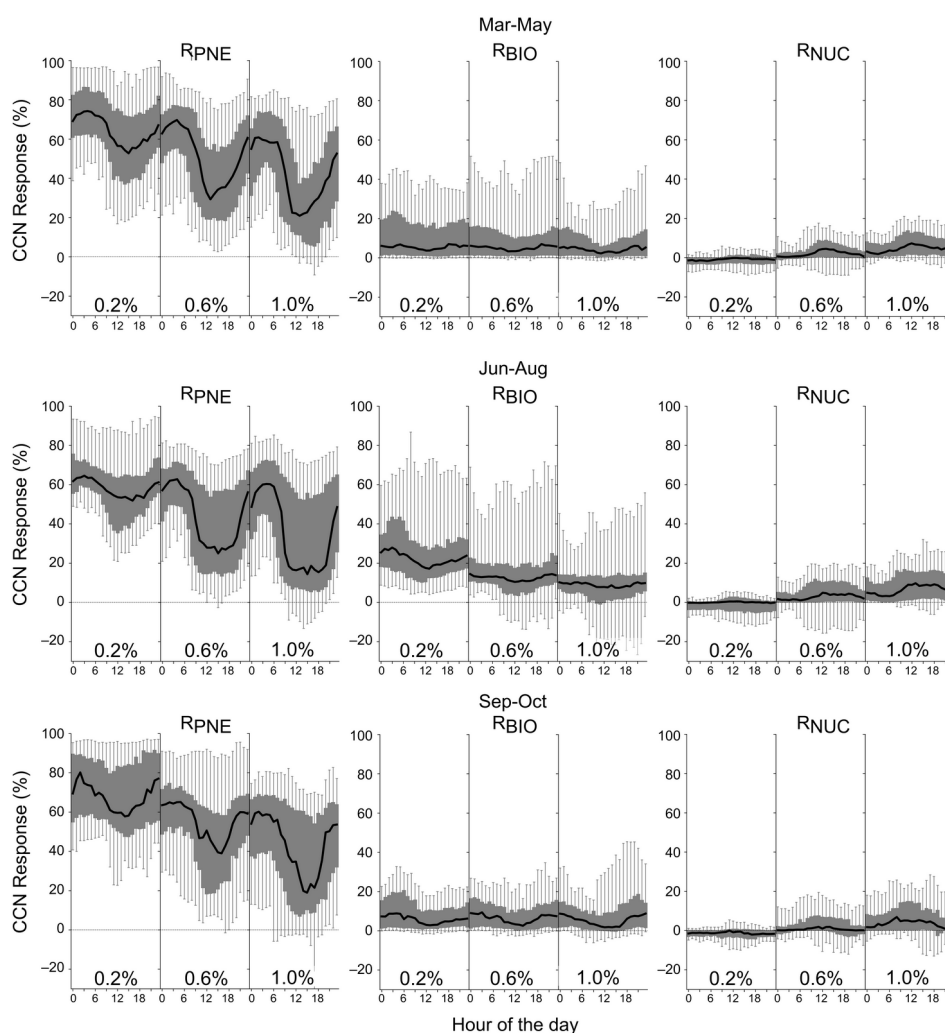


Figure 19: Diurnal profiles of the CCN responses to changes in anthropogenic particle emissions (left column), BVOC emissions (middle column) and cluster formation rate (right column) at 0.2%, 0.6% and 1.0% supersaturations during spring (top row), summer (middle row) and autumn (bottom row).

References

- 150 Caffrey, P. F., Ondov, J. M., Zuffall, M. J. and Davidson, C. I.: Determination of Size-Dependent Dry Particle Deposition Velocities with Multiple Intrinsic Elemental Tracers, *Environmental Science & Technology*, 32, 1615-1622, 10.1021/es970644f, 1998.
- Farmer, D. K., Boedicker, E. K. and DeBolt, H. M.: Dry Deposition of Atmospheric Aerosols: Approaches, Observations, and Mechanisms, *Ann. Phys. Chem.*, 72, 375-397, 10.1146/annurev-physchem-090519-034936, 2021.
- 155 Gallagher, M., Beswick, K., Duyzer, J., Weststrate, H., Choularton, T. and Hummelshøj, P.: Measurements of aerosol fluxes to speulder forest using a micrometeorological technique, *Atmos. Environ.*, 31, 359-373, 10.1016/s1352-2310(96)00057-x, 1997.

- 160 Gaman, A., Rannik, U., Aalto, P., Pohja, T., Siivola, E., Kulmala, M. and Vesala, T.: Relaxed eddy accumulation system for size-resolved aerosol particle flux measurements, *J. Atmos. Ocean. Tech.*, 21, 933-943, 2004.
- Gordon, M., Staebler, R. M., Liggio, J., Vlasenko, A., Li, S.-M. and Hayden, K.: Aerosol flux measurements above a mixed forest at Borden, Ontario, *Atmos. Chem. Phys.*, 11, 6773-6786, 10.5194/acp-11-6773-2011, 2011.
- 165 Groenholm, T., Launiainen, S., Ahlm, L., Martensson, E. M., Kulmala, M., Vesala, T. and Nilsson, E. D.: Aerosol particle dry deposition to canopy and forest floor measured by two-layer eddy covariance system, *Journal of Geophysical Research: Atmospheres*, 114, D04202, 10.1029/2008JD010663, 2009.
- 170 Grönholm, T., Aalto, P. P., Hiltunen, V., Rannik, Ü., Rinne, J., Laakso, L., Hyvönen, S., Vesala, T. and Kulmala, M.: Measurements of aerosol particle dry deposition velocity using the relaxed eddy accumulation technique, *Tellus B.*, 59, 10.3402/tellusb.v59i3.16998, 2007.
- Grosch, S. & Schmitt, G.: Experimental Investigations on the Deposition of Trace Elements in Forest Areas, in: *Environmental Meteorology*, Springer Netherlands, 201-216, 10.1007/978-94-009-2939-5_15, 1988.
- 175 Höfken, K. D. & Gravenhorst, G.: Deposition of Atmospheric Aerosol Particles to Beech- and Spruce Forest, in: *Deposition of Atmospheric Pollutants*, edited by: , Springer Netherlands, 191-194, 10.1007/978-94-009-7864-5_19, 1982.
- Lavi, A., Farmer, D. K., Segre, E., Moise, T., Rotenberg, E., Jimenez, J. L. and Rudich, Y.: Fluxes of Fine Particles Over a Semi-Arid Pine Forest: Possible Effects of a Complex Terrain, *Aerosol Sci. Technol.*, 47, 906-915, 10.1080/02786826.2013.800940, 2013.
- 180 Lorenz, R. and Murphy, C. E.: Dry deposition of particles to a pine plantation, *Boundary Layer Meteorol.*, 46, 355-366, 10.1007/bf00172241, 1989.
- Mammarella, I., Rannik, U., Aalto, P., Keronen, P., Vesala, T. and Kulmala, M.: Long-term aerosol particle flux observations. Part II: Particle size statistics and deposition velocities, *Atmos. Environ.*, 45, 3794-3805, 10.1016/j.atmosenv.2011.04.022, 2011.
- 185 Möller, U. and Schumann, G.: Mechanisms of transport from the atmosphere to the Earth's surface, *J. Geophys. Res.*, 75, 3013-3019, 10.1029/jc075i015p03013, 1970.
- Paramonov, M., Aalto, P. P., Asmi, A., Prisle, N., Kerminen, V.-M., Kulmala, M. and Petäjä, T.: The analysis of size-segregated cloud condensation nuclei counter (CCNC) data and its implications for cloud droplet activation, *Atmos. Chem. Phys.*, 13, 10285-10301, 10.5194/acp-13-10285-2013, 2013.
- 190 Petters, M. D. and Kreidenweis, S. M.: A single parameter representation of hygroscopic growth and cloud condensation nucleus activity, *Atmos. Chem. Phys.*, 7, 1961-1971, 10.5194/acp-7-1961-2007, 2007.
- 195 Pryor, S.: Size-resolved particle deposition velocities of sub-100 nm diameter particles over a forest, *Atmos. Environ.*, 40, 6192-200, 2006.

- Pryor, S. C., Barthelmie, R. J., Spaulding, A. M., Larsen, S. E. and Petroff, A.: Size-resolved fluxes of sub-100-nm particles over forests, *Journal of Geophysical Research: Atmospheres*, 114, 10.1029/2009jd012248, 2009.
- 200 Pryor, S. C., Gallagher, M., Sievering, H., Larsen, S. E., Barthelmie, R. J., Birsan, F., Nemitz, E., Rinne, J., Kulmala, M., Grönholm, T., Taipale, R. and Vesala, T.: A review of measurement and modelling results of particle atmosphere–surface exchange, *Tellus B: Chemical and Physical Meteorology*, 60, 42, 10.1111/j.1600-0889.2007.00298.x, 2008.
- 205 Qi, J., Yu, Y., Yao, X., Gang, Y. and Gao, H.: Dry deposition fluxes of inorganic nitrogen and phosphorus in atmospheric aerosols over the Marginal Seas and Northwest Pacific, *Atmos. Res.*, 245, 105076, 10.1016/j.atmosres.2020.105076, 2020.
- Sehmel, G.: Particle eddy diffusivities and deposition velocities for isothermal flow and smooth surfaces, *J. Aerosol Sci.*, 4(2), 125–38, 1973.
- 210 Simpson, D., Benedictow, A., Berge, H., Bergström, R., Emberson, L. D., Fagerli, H., Flechard, C. R., Hayman, G. D., Gauss, M., Jonson, J. E., Jenkin, M. E., Nyíri, A., Richter, C., Semeena, V. S., Tsyro, S., Tuovinen, J.-P., Valdebenito, Á. and Wind, P.: The EMEP MSC-W chemical transport model – technical description, *Atmos. Chem. Phys.*, 12, 7825–7865, 10.5194/acp-12-7825-2012, 2012.
- 215 Vong, R. J., Vong, I. J., Vickers, D. and Covert, D. S.: Size-dependent aerosol deposition velocities during BEARPEX’07, *Atmos. Chem. Phys.*, 10, 5749–5758, 10.5194/acp-10-5749-2010, 2010.
- Waraghai, A. & Gravenhorst, G.: Dry Deposition of Atmospheric Particles to an Old Spruce Stand, in: *Mechanisms and Effects of Pollutant-Transfer into Forests*, edited by: , Springer Netherlands, 77–86, 10.1007/978-94-009-1023-2_9, 1989.
- 220 Yu, S., Eder, B., Dennis, R., Chu, S. and Schwartz, S. E.: New unbiased symmetric metrics for evaluation of air quality models, *Atmos. Sci. Lett.*, 7, 26–34, 10.1002/asl.125, 2006.
- 225 Zhang, X., Cappa, C. D., Jathar, S. H., McVay, R. C., Ensberg, J. J., Kleeman, M. J. and Seinfeld, J. H.: Influence of vapor wall loss in laboratory chambers on yields of secondary organic aerosol, *Proc. Natl. Acad. Sci.*, 111, 5802–5807, <https://doi.org/10.1073/pnas.1404727111>, 2014.
- Zufall, M., Davidson, C., Caffrey, P. and Ondov, J.: Airborne concentrations and dry deposition fluxes of particulate species to surrogate surfaces deployed in southern Lake Michigan., *Environ. Sci. Technol.*, 32, 1623–28, 1998.